Supporting Information for

Archaeomagnetism in the Levant and Mesopotamia reveals the largest changes in the geomagnetic field

Ron Shaar[1], Yves Gallet[2], Yoav Vaknin[1,3], Lilach Gonen[1], Mario A. S. Martin[3], Matthew J. Adams[4] , Israel Finkelstein[3,5]

[1] The Institute of Earth Sciences, The Hebrew University of Jerusalem, Jerusalem, 91904, Israel

[2] Université Paris Cité, Institut de Physique du Globe de Paris, CNRS, 75005, Paris, France

[3] Institute of Archaeology of Tel Aviv University, Tel Aviv 6997801, Israel

[4] W.F. Albright Institute of Archaeological Research, Jerusalem, Israel

[5] School of Archaeology and Maritime Cultures, University of Haifa, Haifa, Israel

Contents of this file

Text S1 to S4
Tables S4 to S9
Figure S1

Additional Supporting Information (Files uploaded separately)

Table S1: Supplementary archaeological information
Table S2: Specimen archaeointensity data
Table S3: Samples archaeointensity data
Table S10: LAC.v.1.0 data input file
Table S11 LAC.v.1.0 Bayesian curve

Introduction

This supporting information file includes additional text and tables associated with re-analysis of published data: an update on the archaeological ages and new divisions of the previously published samples to 'groups',

- Tel Hazor: Text S1, Tables S4-S5

- Timna-30: Text S2, Tables S6-S8
- Stamped Judean jars: Text S3, Tables S9
- Syrian fragment groups: Text S4

Text S1. Revisions and updates to published archaeomagnetic data from Tel Hazor

Tel Hazor archaeointensity results are similar to those published in Shaar et al. (2016). Yet, in Shaar et al. (2016) we did not divide the data from strata V-VI to phases. Here, we split strata V-VI to three distinct groups according to the corresponding archaeological phases. The three phases are stratigraphically ordered within one excavation area and end in the historically-dated Assyrian destruction of Tel-Hazor (the same destruction of Tel Megiddo). Therefore, these contexts are treated in the model as firm historically-constrained ages (colored symbols in Fig. 6 main text). The ages of the groups are shown in Table S3. Table S4 shows the published archaeointensity data from Tel Hazor calculated as group means.

Text S2. Revisions and updates to published archaeomagnetic data from Timna-30

The original data from Shaar et al. (2011) were re-interpreted in Shaar et al. (2016) using the same interpretation method and selection criteria used here and in Shaar et al. (2020); Shaar et al. (2016). Here, these samples are grouped according to slag layers. All layers, except layer 0 consist of at least three samples. The data in layer 6 is clustered in two sub-groups of samples: one group with two samples that have paleointensity > 90 μT, and a second group with three samples that have paleointensity < 80 μT. The groups means are given in Table S5.

The age model of Timna-30 slag mound was originally based on magnetostratigraphic correlation with radiocarbon ages of Khirbet en-Nahas (KEN) (Ben-Yosef et al., 2009; Levy et al., 2008). However, the archaeointensity analysis in KEN did not follow all the procedures, which have become standard in later studies, and as a result, almost all slag samples from KEN fail the selection criteria used in LAC.v.1.0. We therefore revert to the age model of Timna-30 that uses the five radiocarbon dates from Timna-30 slag mound only (Fig. S1 and Table S1 in Shaar et al., 2011, supplementary material). As the published ages in Shaar et al. (2011) were calibrated using an older radiocarbon calibration curve, we recalibrate them here using the latest IntCal20 (Reimer et al., 2020) (Table S6). Bayesian age model was calculated with Oxcal program using "Sequence" command to account for the stratigraphic constraints. The ages of the slag layers from which the organic samples were collected (i.e. layer "8", Fig. 3 in Shaar et al., 2011) are the modeled ages shown in Table S7. The ages of the other layers (ten slag layers and nine sterile layers between the slag layers) are extrapolated evenly between the dated layers and shown in Table S8.

Text S3. Revisions and updates to Judean stamped handles data

Data of Judean stamped handles from Ben-Yosef et al. (2017) and Vaknin et al. (submitted) are grouped following Vaknin et al. (submitted). The groups data are given in Table S8.

Text S4. Revisions and updates to Judean stamped handles data

The ages of the following groups of pottery fragments previously published in Gallet et al. (2006) and Genevey et al. (2003) have been updated to take into account more recent findings (Masetti-Rouault, 2016):

- The age of group Lot 05 is updated to 1275-1150
- The age of group TM01 is updated to 803-775
- The age of group Lot 28 is updated to 820-765
- The age of group Lot 29 is updated to 750-650

In addition,

- The age of group SY46 from Ebla is updated to 2300-2000 BCE to be consistent with other groups from close contexts (SY53-SY54-SY55)

The ages of the results obtained from Tell Atij and Tell Gudeda (Gallet et al., 2020) are updated to 2750 +/- 175 BCE and 2437.5 +/- 137.5 BCE, respectively, and further constrained by their time-order relationship. This option allows us to consider no a priori on the accumulation rates across the two archaeological sequences (see Gallet et al. (2020) for details)

Stratum/Phase	Samples	New age range
Hazor-V-B (hz05-B)	hz05a,hz05,hz05d,hz05	-800, -750
Hazor-V-C (hz05-C)	hz05b,hz05e,hz05g,hz05h	-815, -765
Hazor-VI (hz06)	hz06a, hz06b, hz06c	-830, -780

Table S4. Archaeointensity grouping of strata Hazor V-VI.

Group name	Stratum	N fragments	n specimens	B (μT)	B σ (μT)	VADM (ZAm^2)	VADM σ (ZAm^2)	Age	Age σ
hz20	Hazor XX	4	16	38.1	5.3	71.6	9.9	-2650	150
hz18 *	Hazor XVIII	3	12	46.9	1.1	88.2	2.1	-2275	75
HZ17F	Hazor XVII-F	4	15	39.8	2.5	74.8	4.6	-1785	100
HZ17E	Hazor XVII-E	3	13	37.5	1.7	70.5	3.3	-1755	100
HZ17D	Hazor XVII-D	3	15	39.8	2.5	74.9	4.8	-1720	100
HZ16C	Hazor XVI-C	4	16	38.1	3.3	71.7	6.1	-1680	112.5
HZ16B	Hazor XVI-B	4	16	39.2	3.5	73.7	6.6	-1640	112.5
HZ16A	Hazor XVI-A	4	17	39.7	4.1	74.7	7.7	-1600	112.5
hz15	Hazor XV	3	9	49.9	0.5	93.8	1	-1550	100
hz13 †	Hazor XIII	4	21	58	2.5	109.1	4.7	-1250	50
hz11	Hazor XI	3	10	63	4.8	118.5	8.9	-1100	100
hz10	Hazor X	2	8	67.3	0.4	126.5	0.7	-950	50
hz07	Hazor VII	5	23	67.8	6.9	127.5	13	-850	50
hz06	Hazor VI	3	15	72.1	5.1	135.5	9.6	-805	25
hz05-C	Hazor V-C	4	23	71.3	4	134.2	7.5	-790	25
hz05-B	Hazor V-B	3	15	84.3	3.5	158.5	6.5	-775	25

* Based on unpublished radiocarbon ages
† Age based on radiocarbon data (Lev et al., 2021)

Table S5. Tel Hazor archaeointensity groups data used in LAC.v.1.0.

Layer	Group name	N fragments	n specimens	B (μT)	B σ (μT)	VADM (ZAm^2)	VADM σ (ZAm^2)
9	Timna30-09	3	13	75.2	3.8	147.5	7.4
8	Timna30-08	3	12	68.9	2.4	135.2	4.7
7	Timna30-07	4	18	73.7	3.7	144.5	7.3
6	Timna30-06-spikes	2	8	92.6	3.8	181.6	7.5
6	Timna30-06	3	14	71.4	2.3	140	4.5
5	Timna30-05	4	18	72.6	6.7	142.4	13.2
4	Timna30-04	3	9	71.5	1.4	140.2	2.8
3	Timna30-03	3	12	74.5	4.3	146.1	8.4
2	Timna30-02	3	16	68.2	2.7	133.7	5.3
1	Timna30-01	4	16	68.8	4.7	134.8	9.2
0	Timna30-00	2	7	81	0.4	158.8	0.8

Table S6. Timna-30 group archaeointensity.

		Unmodeled Age (BCE)							Modeled Age (BCE)						
Sample	14C age	From (68.3%)	To (68.3%)	From (95.4%)	To (95.4%)	μ	median	σ	From (68.3%)	To (68.3%)	From (95.4%)	To (95.4%)	μ	median	σ
S1-w7	2859 ± 34	-1108	-937	-1184	-919	-1029	-1028	59	-1106	-1009	-1126	-939	-1050	-1046	45
S1-d3	2893 ± 39	-1155	-1009	-1213	-936	-1082	-1079	65	-1057	-985	-1095	-934	-1021	-1021	38
S1-g1	2819 ± 35	-1012	-922	-1109	-851	-974	-972	51	-1011	-944	-1040	-919	-977	-979	31
S2-g1	2814 ± 34	-1008	-923	-1103	-841	-968	-967	48	-967	-909	-1008	-895	-942	-940	30
S2-W1	2705 ± 35	-898	-812	-916	-804	-859	-857	34	-916	-828	-971	-807	-880	-884	36

Table S7. Timna-30 radiocarbon data.

Layer	From (68.3%)	To (68.3%)	From (95.4%)	To (95.4%)	μ	median	σ
0	-890	-788	-952	-763	-849	-856	39
1	-942	-868	-990	-851	-911	-912	33
2	-973	-914	-1013	-898	-947	-946	30
3	-986	-924	-1022	-905	-957	-957	30
4	-998	-934	-1031	-912	-967	-968	31
5	-1005	-939	-1035	-916	-972	-973	31
6	-1042	-971	-1077	-929	-1006	-1007	36
7	-1073	-993	-1105	-936	-1031	-1029	40
8	-1106	-1009	-1126	-939	-1050	-1046	45
9	-1139	-1025	-1147	-942	-1069	-1063	50

Table S8. Modeled radiocarbon ages of the slag layers in Timna-30 slag mound.

Group name	Age range	N fragments	n specimens	B (µT)	B σ (µT)	VADM (ZAm^2)	VADM σ (ZAm^2)
lmlk_old	-800, -701	4	12	73.8	9.5	141.2	18.1
Private_Stamp	-800, -701	3	11	72.6	4.3	138.9	8.2
lmlk_young[a]	-701, -630	7	24	69.7	5.3	133.2	10.1
Rosette	-660, -586	2	7	71.9	0.6	137.3	1.2
Lion[a]	-586, -520	3	11	65.8	2.1	125.7	4.1

Table S9. Archaeointensity group data of the Judean handles. Age ranges are slightly different than those in Ben-Yosef et al. (2017) and are based on Vaknin et al. (submitted).
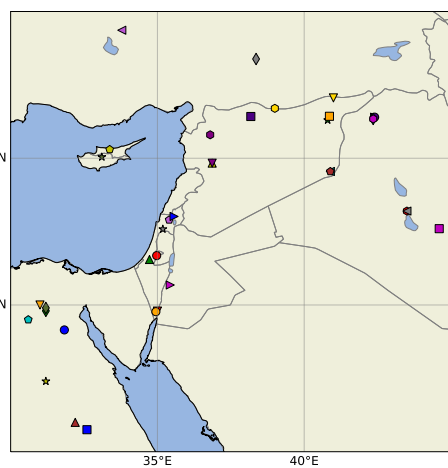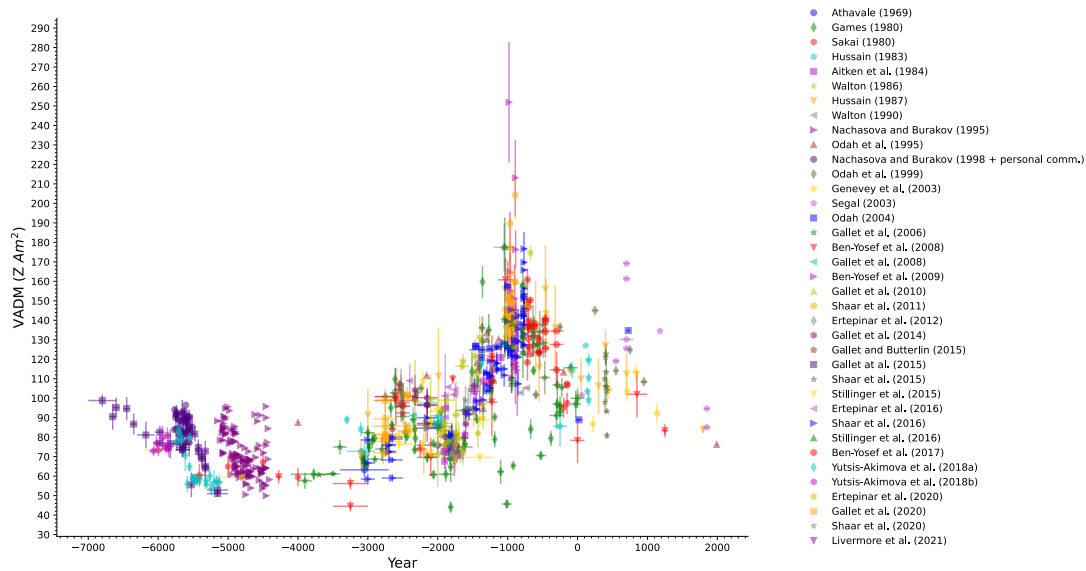
Figure S1: All archaeointensity data published from 1969-2021 in the locations shown on the map.

References

Ben-Yosef, E., Millman, M., Shaar, R., Tauxe, L., & Lipschits, O. (2017). Six centuries of geomagnetic intensity variations recorded by royal Judean stamped jar handles. *Proceedings of the National Academy of Sciences of the United States of America, 114*(9), 2160-2165 https://doi.org/10.1073/pnas.1615797114

Ben-Yosef, E., Tauxe, L., Levy, T. E., Shaar, R., Ron, H., & Najjar, M. (2009). Geomagnetic intensity spike recorded in high resolution slag deposit in Southern Jordan. *Earth and Planetary Science Letters, 287*(3-4), 529-539 https://doi.org/10.1016/j.epsl.2009.09.001

Gallet, Y., Fortin, M., Fournier, A., Le Goff, M., & Livermore, P. (2020). Analysis of geomagnetic field intensity variations in Mesopotamia during the third millennium BC with archeological implications. *Earth and Planetary Science Letters, 537* https://doi.org/10.1016/j.epsl.2020.116183

Gallet, Y., Genevey, A., Le Goff, M., Fluteau, F., & Ali Eshraghi, S. (2006). Possible impact of the Earth's magnetic field on the history of ancient civilizations. *Earth and Planetary Science Letters, 246*(1-2), 17-26 https://doi.org/10.1016/j.epsl.2006.04.001

Genevey, A. S., Gallet, Y., & Margueron, J. C. (2003). Eight thousand years of geomagnetic field intensity variations in the eastern Mediterranean. *Journal of Geophysical Research-Solid Earth, 108*(B5) https://doi.org/10.1029/2001jb001612

Lev, R., Bechar, S., & Boaretto, E. (2021). Hazor EB III city abandonment and IBA people return: radiocarbon chronology and its implications. *Radiocarbon, 63*(5), 1453-1469 https://doi.org/10.1017/RDC.2021.76

Levy, T. E., Higham, T., Ramsey, C. B., Smith, N. G., Ben-Yosef, E., Robinson, M., et al. (2008). High-precision radiocarbon dating and historical biblical archaeology in southern Jordan. *Proceedings of the National Academy of Sciences of the United States of America, 105*(43), 16460-16465 https://doi.org/10.1073/pnas.0804950105

Masetti-Rouault, M. G. (2016). Assyrian colonization in Eastern Syria: the case of Tell Masaikh (ancient Kar-Ashurnasirpal). In J. MacGinnis, D. Wicke, T. Greenfield, & A. Stone (Eds.), *The provincial archaeology of the Assyrian empire* (pp. 199-212): MacDonald institute monograph.

Reimer, P. J., Austin, W. E. N., Bard, E., Bayliss, A., Blackwell, P. G., Ramsey, C. B., et al. (2020). The Intcal20 Northern hemisphere radiocarbon age calibration curve (0-55 Cal Kbp). *Radiocarbon, 62*(4), 725-757 https://doi.org/10.1017/Rdc.2020.41

Shaar, R., Bechar, S., Finkelstein, I., Gallet, Y., Martin, M. A. S., Ebert, Y., et al. (2020). Synchronizing Geomagnetic Field Intensity Records in the Levant Between the 23rd and 15th Centuries BCE: Chronological and Methodological Implications. *Geochemistry Geophysics Geosystems, 21*(12) https://doi.org/10.1029/2020GC009251

Shaar, R., Ben-Yosef, E., Ron, H., Tauxe, L., Agnon, A., & Kessel, R. (2011). Geomagnetic field intensity: How high can it get? How fast can it change?

Constraints from Iron Age copper slag. *Earth and Planetary Science Letters, 301*(1-2), 297-306 https://doi.org/10.1016/j.epsl.2010.11.013

Shaar, R., Tauxe, L., Ron, H., Ebert, Y., Zuckerman, S., Finkelstein, I., & Agnon, A. (2016). Large geomagnetic field anomalies revealed in Bronze to Iron Age archeomagnetic data from Tel Megiddo and Tel Hazor, Israel. *Earth and Planetary Science Letters, 442*, 173-185 https://doi.org/10.1016/j.epsl.2016.02.038

Vaknin, Y., Shaar, R., Lipschits, O., Mazar, A., Maeir, A., Garfinkel, Y., et al. (in press). Reconstructing biblical military campaigns using geomagnetic field data *Proceedings of the National Academy of Sciences*